J. Fluid Mech. (1993), *vol.* 253, *pp.* 1–25

Dynamic simulation of bimodal suspensions of hydrodynamically interacting spherical particles

By CHINGYI CHANG AND ROBERT L. POWELL
Department of Chemical Engineering, University of California, Davis, CA 95616, USA

(Received 10 July 1992 and in revised form 11 November 1992)

Stokesian dynamics is used to simulate the dynamics of a monolayer of a suspension of bimodally distributed spherical particles subjected to simple shearing flow. Hydrodynamic forces only are considered. Many-body far-field effects are calculated using the inverse of the grand mobility matrix. Near-field effects are calculated from the exact equations for the interaction between two unequal-sized spheres. Both the detailed microstructure (e.g. pair-distribution function and cluster formation) and the relative viscosity are determined for bimodal suspensions having particle size ratios of 2 and 4. The flow of an 'infinite' suspension is simulated by considering 25, 49, 64, and 100 particles to be 'one' cell of an infinite periodic array. The effects of both the size ratio and the relative fractions of the different-sized particles are examined. When the area fraction, ϕ_a, is less than 0.4 the particle size distribution does not affect the calculated viscosity. For $\phi_a > 0.4$, and for a fixed fraction of small spheres, the bimodal suspensions generally have lower viscosities than monodispersed suspensions, with the size of this effect increasing with ϕ_a. These results compare favourably with experiment when ϕ_a and the volume fraction, ϕ_v, are normalized by the maximum packing values in two and three dimensions, respectively. At the microstructural level, viscosity reduction is related to the influence of particle size distribution on the average number of particles in clusters. At a fixed area fraction, the presence of smaller particles tends to reduce average cluster size, particularly at larger ϕ_a, where significant viscosity reductions are observed. Since the presence of large clusters in monodispersed suspensions has been directly linked to high viscosities, this provides a dynamic mechanism for the viscosity reduction in bimodal suspensions.

1. Introduction

Determination of the rheological properties and other microstructural transport properties for suspensions of monodispersed spherical particles has been the principal goal of many theoretical and experimental studies. Such systems are often considered as providing models of many industrially important materials such as coal–water mixtures, paints, coatings, and polymer emulsions. In a somewhat smaller, but significant, class of suspensions, functional performance is linked to the total amount of solids. For example a typical hydroxy-terminated polybutadene solid rocket fuel consists of ammonium perchlorate and aluminium particles in a rubbery binder (Miller, Lee & Powell 1991). The total available energy for propulsion is directly linked to the amount of solids present. During processing, such a fuel is actually a highly loaded suspension having volume fractions exceeding the maximum random packing for monodispersed suspensions. As an example, the Advanced Solid Rocket Motor currently under development by the National Aeronautics and Space Administration

will contain over 75% solids by volume. On a much smaller scale, dental pastes can also contain high volume loadings of a solid component such as crushed glass (Cheng *et al.* 1990). In such cases where high volume loadings are desired, the concomitant high viscosity is usually not favourable from a processing standpoint. However, high solids loadings can be attained with a small increase in viscosity using suspensions having a distribution of particle sizes rather than particles of similar sizes. From a practical and experimental standpoint, this effect is well-known. The purpose of this paper is to apply theoretical fluid mechanics and modern simulation techniques, namely Stokesian dynamics, to directly predict the observed viscosity reduction as well as the flow-induced microstructure. Our results apply to systems in which Brownian and surface forces are negligible and hydrodynamic forces dominate (Johma *et al.* 1991).

The first systematic study of the effect of modality on suspension rheology is due to Sweeny & Geckler (1954). A concentric cylinder viscometer was used to measure the viscosity of bimodally dispersed suspensions of glass spheres in an aqueous glycerol and zinc bromide medium. The size ratio, λ (the ratio of the diameter of large spheres, d_l, to the diameter of small spheres, d_s), was varied from 1 to 20.76, with d_l being fixed at 262 μm while d_s was systematically reduced to 12 μm. The overall volume fraction in each suspension, ϕ_v, was 0.55. The volume fraction of spheres having the smaller diameter, $\xi\phi_v$, was fixed with $\xi = 0.25$. As λ increased, the viscosity at low shear rates (i.e. the range of shear rates over which the viscosity is constant) decreased, until, for $\lambda = 20.76$, the viscosity was less than 25% of that for a monodispersed suspension. Working at lower volume fractions, Eveson (1959) also used a Couette viscometer to measure the viscosity of bimodal suspensions of polymethyl methacrylate spheres with $d_s = 4.7$ μm and $d_l = 190$ and 390 μm. He observed a less than 5% change in relative viscosity for volume fractions of solids as high as 0.20 when $\lambda \leqslant 8$. He concluded that the reduction in relative viscosity for a bimodal suspension becomes significant, that is, reproducibly measurable, only when $\phi_v > 0.175$ and when λ was the maximum used, $\lambda = 8$. He also found that for ϕ_v fixed, the viscosity decreased as ξ increased from zero, reached a minimum at some value of ξ less than or equal to 0.5 and then increased as $\xi \to 1$.

Over a decade later, an extensive investigation of the rheological behaviour of multimodal suspensions of glass spheres was reported by Chong, Christiansen & Baer (1971). They used an orifice viscometer in which the suspensions are driven through an abrupt contraction. The pressure drop and flow rate were measured and used to calculate the viscosity. The advantage of such a system is that fluid layers do not form near the orifice walls. Such effects, which can also be interpreted as wall slippage, are observed when concentrated suspensions are tested in capillary and rotational viscometers. Figure 1 reproduces the principal results of their study which confirmed the earlier findings (Sweeny & Geckler 1954; Eveson 1959). It depicts the dependence of the relative viscosities of bimodal suspensions on the particle size ratios and the overall volume fraction with the fraction of small spheres of total solids being maintained at 0.25. Also given are data for suspensions of monodispersed spheres. At high volume fractions, near the maximum packing for monodispersed suspensions, bimodal suspensions show a dramatically lower viscosity than monodispersed suspensions. Above these volume fractions, where a 'suspension' consisting of single-sized particles would appear to be a wet granular solid, a bimodal suspension can behave as a fluid having a relative viscosity, η_r, of less than 100. The size of the viscosity reduction increases with ϕ_v and with λ. For example, at $\phi_v = 0.58$, the relative viscosities for suspensions with size ratio 1.0 (monodispersed), 2.1, 3.19, and 7.25 are

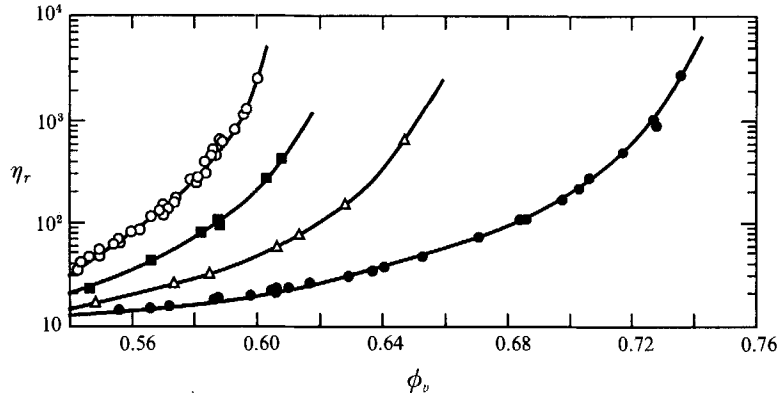

FIGURE 1. Dependence of relative viscosity on volume fraction and particle size ratio, λ (from Chong *et al.* 1971): ○, monodispersed, $\lambda = 1$; ■, $\lambda = 2.1$; △, $\lambda = 3.19$; ●, $\lambda = 7.25$. The fraction of small spheres, ξ, is fixed at 0.25.

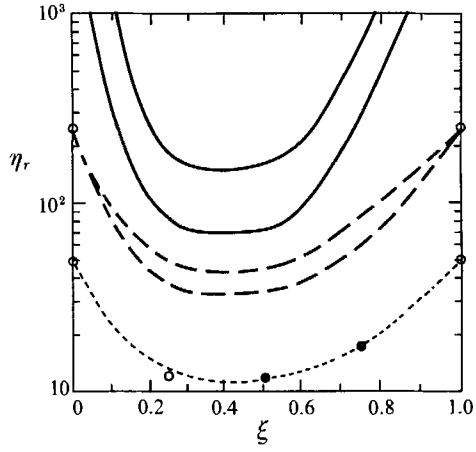

FIGURE 2. Calculated viscosities showing dependence of relative viscosity upon λ, and fraction of small spheres, ξ, for bimodal suspensions of spheres. ●, Data of Chong *et al.* (1971); ○, data of Sweeny & Geckler (1954). Estimates using (1.1): ——, $\phi_v = 0.65$, $\lambda = 7.3$ (top) and 22.2 (bottom); — —, $\phi_v = 0.60$, $\lambda = 2.7$ (top) and 7.3 (bottom).

approximately 300, 80, 30, and 15 respectively. At $\phi_v = 0.64$, $\lambda = 1$ and 2.1 data for η_r are not given, implying that they could not be measured, while for $\lambda = 3.19$ and 7.25, $\eta_r \approx 300$ and 30, respectively.

Chong *et al.* (1971) recast their data, as well as those of Sweeny & Geckler (1954), in terms of the relative viscosity as a function of ξ for various λ and ϕ_v, see figure 2. In arriving at this reformulation, the original data were correlated using

$$\eta_r = \left[1 + 0.75\left(\frac{\phi_v/\phi_m^{3d}}{1-\phi_v/\phi_m^{3d}}\right)\right]^2, \tag{1.1}$$

where ϕ_m^{3d} is the maximum packing in three dimensions, which besides the physical geometrical arrangement depends upon both λ and ξ. To construct figure 2, a value of λ is chosen. Then, for each ξ, ϕ_m^{3d} is determined from empirical correlations and η_r versus ϕ_v is found. Repeating this procedure allows the dependence of η_r upon ξ to be ascertained. Equation (1.1) reduces to the Einstein equation as $\phi_v \to 0$ if $\phi_m^{3d} = 0.60$. For

bimodal suspensions, ϕ_m^{3d} was determined empirically using a graphical technique based upon the notion that η_r approaches infinity as $\phi_v \to \phi_m^{3d}$ (Chong *et al.* 1971). Figure 2 shows that there are parameter ranges where a small change in suspension composition, that is ξ, causes a large variation in viscosity. However, for smaller size ratios and lower volume fractions, even relatively large changes in ξ cause little variation. Figure 2 also shows that the minimum viscosity of a bimodal system can be achieved with 25% to 35% small spheres. These results are supported by the recent study of Shapiro & Probstein (1992) who measured the random close-packing volume fractions for monomodal and bimodal suspensions ($\lambda = 2$ and 4) as a function of ξ. The curves for ϕ_m^{3d} versus ξ are analogous to those shown in figure 2, but inverted. That is, the maximum ϕ_m^{3d} for a bimodal suspension may be achieved with $\xi = 0.25$ to 0.4. Overall their study strongly suggests that in bimodal suspensions, η_r at high volume fractions is directly linked to the value of ϕ_m^{3d} associated with a particular size ratio and small sphere fraction.

Other studies have tended to support the earlier work while extending its range and identifying potential experimental pitfalls. Using a capillary viscometer, Goto & Kuno (1982, 1984) showed large decreases in the relative viscosity for bimodal suspensions even when $\phi_v \approx 0.2$. However, they attributed much of this reduction to particle–wall interactions. In particular, they found the largest reduction when d_l was large relative to the diameter of the capillary. Storms, Ramarao & Weiland (1990) measured the viscosity for suspensions of bimodally distributed polymethyl methacrylate (PMMA) beads dispersed in silicone oil using an orifice viscometer similar to that of Chong *et al.* (1971). As with the earlier study, their data apply at high Péclet numbers, $O(10^6$–$10^7)$, but at sufficiently low shear rates that the viscosity is independent of shear rate. Here, the Péclet number, Pe is $6\pi\mu a^3\dot{\gamma}/kT$, where μ is the suspending fluid viscosity, a is the particle radius, $\dot{\gamma}$ is the shear rate, k is Boltzmann's constant and T is temperature. They expanded the earlier work sufficiently to be able to quantitatively determine the effects of λ and ξ upon the viscosity of bimodal suspensions. They proposed an expression of the form

$$\eta_r = \left(1 + \frac{R\phi_v}{1 - \phi_v/\phi_m^{3d}}\right)^{3.3\phi_m^{3d}}, \tag{1.2}$$

where R varies from 0.7 to 1.25 depending upon ξ and λ and is tabulated in their paper; ϕ_m^{3d} is determined from a series of algebraic expressions that also depend upon ξ and λ.

Poslinski *et al.* (1988) examined the rheology of suspensions of bimodal particles in a polybutene oil that is Newtonian at room temperature using a parallel-plate viscometer. All measured properties, including the shear viscosity, primary normal stress coefficient, dynamic viscosity, and storage modulus were lower for a bimodal suspension than for a suspension having a monomodal size distribution of particles.

Finally, the most recent study dealing with bimodal suspensions of non-colloidal and non-Brownian particles is due to Shapiro & Probstein (1992). They used a Couette viscometer to determine the viscosity of monomodal and bimodal suspensions of glass beads (40–160 μm) in a 95% glycerin/5% water solution. To avoid wall slippage, they took measurements at low shear rates where the viscosity is independent of the shear rate, but the Péclet number is still large, $O(10^7)$. They found differences in η_r between the $\lambda = 1$ suspensions and the bimodal case with $\lambda = 4$ and $\xi = 0.5$ when $\phi_v \geqslant 0.15$.

For suspensions having sufficiently high solids loading to make multimodal effects important, the experimental findings can be summarized in two parts. First, when ϕ_v

and ξ are fixed, η_r depends upon λ and decreases with increasing λ. Second, when ϕ_v and λ are fixed, η_r depends upon ξ, decreasing as ξ increases from zero, reaching a minimum for ξ around 0.25 and increasing as $\xi \to 1$.

Theoretically describing the effect of bimodal populations of spherical particles on the macroscopic rheology has only been attempted in the limiting case when the size ratio is large. Farris (1968) developed an 'effective medium' model in which the small particles in suspension were viewed as a continuum with respect to the larger ones. He showed that when $\lambda \geqslant 10$, it is possible to estimate the viscosity of a multimodal suspension from the viscosity–concentration behaviour of a monomodal suspension, considering the fine particles as a homogeneous phase. This model does not account for the fluid mechanical interactions and it does not attempt to elucidate microstructural information. The viscosity of a bimodal suspension of spheres is calculated by treating the mixture of fine particles and suspending fluid as a 'homogeneous' fluid. This comprises a volume V_0 of suspending liquid and V_s of fines and has a viscosity of

$$\eta_1 = h(\phi_1)\,\mu, \tag{1.3}$$

where ϕ_1 is the volume fraction of fines in the suspending fluid/fines mixture,

$$\phi_1 = \frac{V_s}{V_s + V_0} = \frac{\xi \phi_v}{1 + (\xi - 1)\,\phi_v}, \tag{1.4}$$

and h is a function that is either determined empirically, theoretically or from simulations. The coarse particles are considered to be suspended in a 'homogeneous' fluid consisting of the fines and suspending fluid. The relative viscosity of this suspension is

$$\eta_r = h(\phi_2)\,\eta_1/\mu = h(\phi_2)\,h(\phi_1), \tag{1.5}$$

where $\phi_2 = (1 - \xi)\,\phi_v$. A similar procedure can be followed for multimodal suspensions, in general (Farris 1968).

More recently, Sengun & Probstein (1989*a*) used a model similar to that of Farris (1968) to predict the rheological behaviour of stable slurries which were composed of a coarse fraction (100–300 μm) and a fine fraction in the colloidal size range (2–3 μm). They use a decomposition similar to (1.3)–(1.5), except that the viscosity can exhibit non-Newtonian, that is, shear thinning, effects due to the colloidal fraction. This is similar to the model of Chan & Powell (1984) that predicts the linear viscoelastic properties of suspensions of spheres in non-Newtonian fluids.

When the size ratio is not large, particle–particle interactions must be directly considered in any theory of the rheology of bimodal suspensions. Large effects on the viscosity are found experimentally even when $\lambda \approx 3$, in which case an effective medium theory would not be expected to hold. Further, since measured effects generally occur at high volume fractions, the theoretical construct must allow modelling under such circumstances. Dynamic computer simulation offers a powerful tool to study multimodal suspensions of particles hydrodynamically interacting in the Stokes' flow regime (Barnes, Edwards & Woodcock 1987). Macroscopic suspension properties, such as effective viscosity, sedimentation rate or self-diffusion coefficient can be determined through appropriate temporal and spatial averaging of microstructural information. One such technique, termed Stokesian dynamics (Brady & Bossis 1988), uses a molecular-type approach to follow the time evolution of the positions of particles in suspension undergoing an imposed flow. This technique, which is related to the multipole-moment method (Weinbaum, Ganatos & Yan 1990), has two singular features that enhance its ability to deal with highly concentrated suspensions: the

inversion of the grand mobility matrix to obtain the grand resistance tensor (which describes many-body interactions); and the inclusion of near-field lubrication effects. The grand mobility matrix, which describes the velocity disturbance produced by a few lowest-order multipoles representing each sphere, does not contain the reflections of the other spheres required to describe the screening effects associated with many-body interactions. Yet its inverse, the grand resistance matrix, appears to sum all the multiple reflections of these lowest-order multipoles. Durlofsky, Brady & Bossis (1987) computed the resistance interaction along the line of centres of two spheres and illustrated this important point, that is, the equivalence of inverting mobility matrix and summing reflected interactions.

Lubrication forces between neighbouring spheres are calculated using the exact formulas for the interaction of two spheres. Far-field effects are then subtracted from these formulae to eliminate 'double accounting' of far-field effects which otherwise occurs due to their inclusion in the mobility matrix. Stokesian dynamics has elucidated several mechanisms in flows such as sedimentation and simple shearing. The results obtained so far using this method, however, are for monodispersed suspensions only.

In this paper, we report upon both micro- and macro-rheological properties of suspensions of unequal-sized spheres that are determined using Stokesian dynamics. Following the procedure developed by Durlofsky *et al.* (1987), in §2 we present a general method for computing the hydrodynamic interactions among N spherical particles of two different sizes. We form the N-sphere mobility matrix for unequal-sized spheres in terms of a moment expansion, and adjust its invert for lubrication. We specialize these results to a monolayer of bimodal rigid non-Brownian, non-colloidal spheres in a simple shearing flow. Hence, our theory applies to the case $Pe \to \infty$. Equations are developed to compute the trajectory of the particles and the effective viscosity for bimodal suspensions from the instantaneous and time-averaged bulk stress (Batchelor 1970). In a monolayer, all particles lie in the same plane, the plane of shear. As discussed in Brady & Bossis (1985), examining a sheared monolayer rather than a full three-dimensional suspension minimizes the computation costs (reducing the number of degrees of freedom for each sphere from eleven to six) while preserving the essential physics in the plane of shear.

In § 3 we present simulation results for the detailed microstructure (pair-distribution function and cluster formation) and the macroscopic rheology (relative viscosity) of bimodal suspensions. Our numerical results suggest that the viscosity reduction in bimodal suspensions is linked to the influence of particle size distribution and the relative fractions of the two particle populations on cluster formation. At a fixed volume fraction, the presence of small spheres tends to reduce the average cluster size in a suspension. Since large clusters in monodispersed suspensions have been directly linked to high viscosities (Bossis & Brady 1989), this would provide a dynamic mechanism for the viscosity reduction in bimodal suspensions. We also compare our numerically determined suspension viscosities with experimental results. These comparisons illustrate the accuracy of the general method and also demonstrate the ability of the Stokesian dynamics to handle highly concentrated suspensions of unequal-sized spheres. Finally, we summarize our principal results in §4 and discuss possible extensions of the simulation method for bimodal suspensions, such as the inclusion of colloidal forces.

2. Method

The application of the multipole-moment technique to Stokesian dynamics is discussed by Durlofsky *et al.* (1987) and Brady & Bossis (1988). Our intent is to develop this methodology further in order to calculate both the microscopic and macroscopic properties of suspensions of unequal-sized spheres. We consider a suspension of N spheres subject to a flow field having an undisturbed velocity U^∞ with a corresponding rate of strain $\boldsymbol{E}^\infty$. The system is finite and consists of two populations of rigid spheres. There are N_1 type-α spheres having radii a and N_2 type-β spheres having radii b. These particles are small enough that the particle Reynolds numbers are much less than unity.

To develop an evolution equation for the suspension microstructure, we follow Durlofsky *et al.* (1987) and write the resistance matrices $\boldsymbol{R}_{FU}$, $\boldsymbol{R}_{FE}$, $\boldsymbol{R}_{SU}$, and $\boldsymbol{R}_{SE}$ as part of a 'grand resistance' matrix, $\boldsymbol{R}$. This permits the force and torque, $\boldsymbol{F}$, and the stresslet, $\boldsymbol{S}$, exerted by the spheres on the fluid to be related to the particle translational and rotational velocities, U, and the rate of strain associated with the imposed flow, $\boldsymbol{E}^\infty$, using

$$\begin{pmatrix} \boldsymbol{F} \\ \boldsymbol{S} \end{pmatrix} = \boldsymbol{R} \begin{pmatrix} U - U^\infty \\ -\boldsymbol{E}^\infty \end{pmatrix}, \tag{2.1}$$

where

$$\boldsymbol{R} = \begin{pmatrix} \boldsymbol{R}_{FU} & \boldsymbol{R}_{FE} \\ \boldsymbol{R}_{SU} & \boldsymbol{R}_{SE} \end{pmatrix}. \tag{2.2}$$

For example, for N particles, $U - U^\infty$ is a vector of dimension $6N$ that contains the translational and rotational velocities of all particles relative to the imposed flow at infinity and evaluated at the centres of the particles; $\boldsymbol{E}^\infty$ is a vector of dimension $5N$ that gives the imposed rate of strain for each particle; $\boldsymbol{F}$ is a $6N$ vector that contains the force and torque exerted by the particles on the fluid; and, S has dimension $5N$ and consists of the particle stresslets. These stresslets result from the symmetric and traceless parts of the first moment of the force distribution integrated over the surfaces of the particles or, more physically, the contribution to the bulk stress due to the existence of the particles. The corresponding inverse or 'grand mobility' matrix, $\boldsymbol{M}$, representation is

$$\begin{pmatrix} U - U^\infty \\ -\boldsymbol{E}^\infty \end{pmatrix} = \begin{pmatrix} \boldsymbol{M}_{UF} & \boldsymbol{M}_{US} \\ \boldsymbol{M}_{EF} & \boldsymbol{M}_{ES} \end{pmatrix} \begin{pmatrix} \boldsymbol{F} \\ \boldsymbol{S} \end{pmatrix}. \tag{2.3}$$

For two unequal-sized spherical particles, the grand resistance and grand mobility matrices are known exactly for all centre–centre separations (Jeffrey & Onishi 1984; Jeffrey & Corless 1988; Corless & Jeffrey 1988; Kim & Karrila 1991; and Jeffrey 1992). For N unequal-sized spheres approximations must be made.

2.1. *Calculation of the grand mobility matrix*: $\boldsymbol{M}^\infty$

Using the multipole-moment method developed by Durlofsky *et al.* (1987), moments are taken of the boundary-integral representation of the velocity field for a bimodal suspension. The zeroth moment is the total force, while the first moment has both a symmetric and an antisymmetric part: the stresslet and torque, respectively. We truncate the expansion after the dipole terms while including two higher multipole contributions (due to a quadruple and an octupole) that result from the finite size of the spheres. The velocity field at any point in the fluid is then related to the forces, torques and stresslets exerted by the unequal-sized spheres on the fluid. The grand mobility matrix, $\boldsymbol{M}^\infty$, is constructed using Faxén's laws (Batchelor & Green 1972). It

relates the translational and angular velocities of each particle relative to the force/torque/stresslet of all N bimodally sized spheres through

$$\begin{pmatrix} U-U^{\infty} \\ -E^{\infty} \end{pmatrix} = M^{\infty} \begin{pmatrix} F \\ S \end{pmatrix}. \tag{2.4}$$

The elements of M^{∞} are given explicitly in the Appendix. In obtaining these expressions, we consider M^{∞} to be the far-field approximation to the interaction among the particles and include terms up to $O(r^{-5})$, where r would reflect a characteristic interparticle spacing. The procedure for inverting M^{∞} to obtain R is equivalent to solving the simultaneous equations (2.4) for the unknown forces, torques and stresslets when the velocities and the ambient rate of strain field are prescribed.

2.2. *Adjustment for near-field effects: lubrication*

The many-body approximation to the resistance matrix (i.e. the invert of M^{∞}) still lacks near-field effects. These would only be reproduced upon inversion of the mobility matrix if all multipole moments were included. To incorporate such lubrication terms, we modify the resistance matrix to include the exact unequal-sized two-sphere formulae of Jeffrey & Onishi (1984); Jeffrey & Corless (1988); Corless & Jeffrey (1988); Jeffrey (1989); Kim & Karrila (1991); and Jeffrey (1992) for the two-body resistance matrix R_{2B}. The modified grand resistance matrix is then written as

$$R = (M^{\infty})^{-1} + R_{2B} - R^{\infty}_{2B}, \tag{2.5}$$

where R^{∞}_{2B} represents the far-field effect of the two-body interaction, which must be subtracted so that it is not included twice in the computation. This is determined by inverting the two-sphere mobility matrix to the same level of approximation as M^{∞}.

2.3. *Calculation of the particle trajectories and the suspension viscosity*

Using (2.5) with (2.1) and (2.2), one can calculate the motion of the particles with prescribed forces and torques in a linear shear flow. The final form of the velocity of the particles is given by

$$U - U^{\infty} = R_{FU}^{-1}[F + R_{FE} : E^{\infty}]. \tag{2.6}$$

Having found the velocities at a given instant, the particle paths are integrated using a predictor–corrector formula (Carnahan, Luther & Wilkes 1969).

In order to determine the rheological properties, we must calculate the bulk stress, $\langle \boldsymbol{\Sigma} \rangle$. The technique for calculating the average or macroscopic stress in homogeneous suspensions has been given by Batchelor (1970, 1977). Since we deal with purely hydrodynamic interactions for neutrally buoyant spheres, $\langle \boldsymbol{\Sigma} \rangle$ here is the average over the volume V containing the $N(= N_1 + N_2)$ particles and is given by

$$\langle \boldsymbol{\Sigma} \rangle = \text{I.T.} + 2\mu E^{\infty} + \left(\frac{1}{V}\right) \cdot S^{H}, \tag{2.7}$$

where

$$S^{H} = \sum_{i=1}^{N_1} S_{\alpha i} + \sum_{i=1}^{N_2} S_{\beta i}.$$

The isotropic term I.T. is of no importance to the rheology of incompressible suspensions. The total particle contributions to the mechanical stress due to the shear flow is S^{H}. The individual contributions, $S_{\alpha i}$, and $S_{\beta i}$, are found by solving (2.1) and (2.2) for the unknown stresslets,

$$S = (R_{SU} \cdot R_{FU}^{-1} \cdot R_{FE} - R_{SE}) : E^{\infty}. \tag{2.8}$$

Here $\boldsymbol{S} = (S_{\alpha 1}, \ldots, S_{\alpha N_1}, S_{\beta 1}, \ldots, S_{\beta N_2})$ is a column vector containing the N-particle stresslets.

Our principal interest is in the relative viscosity of the suspension, η_r, which is the viscosity of the suspension divided by the fluid viscosity. The suspension viscosity is calculated from the (x, y)-component of the stress in a simple shear flow with $u_x^\infty = \dot{\gamma} y$. As with the grand resistance matrix, the stress is non-dimensionalized by $6\pi\mu e^3\dot{\gamma}$, where e is a characteristic length that is the same throughout, for example, $e = \frac{1}{2}(a+b)$. Hence, the relative viscosity is

$$\begin{aligned}\eta_r &= \langle \Sigma_{xy} \rangle / 2\mu E_{xy}^\infty \\ &= 1 + \left(\frac{9e^3}{2a^3}\right)\phi_\alpha \left(\frac{1}{N_1}\right)\sum_{i=1}^{N_1} (S_{\alpha i})_{xy} + \left(\frac{9e^3}{2b^3}\right)\phi_\beta \left(\frac{1}{N_2}\right)\sum_{i=1}^{N_2} (S_{\beta i})_{xy},\end{aligned} \tag{2.9}$$

where ϕ_α and ϕ_β are the volume fractions of the α-type and β-type spheres, respectively. For the monodispersed case, this result can be reduced to

$$\eta_r = 1 + \tfrac{9}{2}\phi_v \left(\frac{1}{N}\right)\sum_{\alpha=1}^{N} (S_\alpha)_{xy}, \tag{2.10}$$

Here, all lengths are non-dimensionalized by the particle radius a.

2.4. *Simulation of a sheared monolayer*

We have simulated the flow of a monolayer of unequal-sized (bimodal) rigid non-Brownian and non-colloidal spherical particles due to an imposed simple shearing flow. All particles lie in the plane of shear, the (x, y)-plane, and particle–particle interactions that result from the macroscopically imposed simple shearing flow all occur in this plane. The bulk rate-of-strain tensor is given by

$$E_{ij}^\infty = \tfrac{1}{2}\dot{\gamma}\begin{bmatrix} 0 & 1 & 0 \\ 1 & 0 & 0 \\ 0 & 0 & 0 \end{bmatrix} \tag{2.11}$$

and the bulk vorticity is

$$\Omega_i = -\tfrac{1}{2}\dot{\gamma}(0, 0, 1). \tag{2.12}$$

There are neither external forces (e.g. gravity) nor external torques (e.g. magnetic field) acting on the particles. In our approach, we model an infinite suspension by periodically replicating the basic unit cell and using periodic boundary conditions. Each particle is centred in its own periodic cell and interacts only with its neighbours in that cell. The basis for this approximation rests with the work of O'Brien (1979). Although hydrodynamic interactions are long-ranged, falling off as r^{-2} for force-free particles (the particles acting like force dipoles), particles outside the periodic cell in total contribute $O(l^{-2})$ to the translational–rotational velocity of the particle at the centre of its periodic cell, where l is a characteristic dimension of the cell (Bossis & Brady 1984; Brady & Bossis 1985). In our case, l is the cell length non-dimensionalized by the radius of a large sphere. Thus, as the size of the periodic cell increases, the effect of particles outside the cell can be made arbitrarily small. Some difficulties arise with the use of periodic boundary conditions to simulate the flow of suspensions of hydrodynamically interacting particles in three dimensions. The mobility matrix may not be positive definite, having negative eigenvalues and inducing imaginary random displacements of the particles (Dickinson 1985). The aphysical result derives from not properly accounting for the long-range interactions. It can be avoided by using the

λ	ξ	N_l	N_s
2	0.073	19	6
2	0.273	10	15
		20	29
2	0.494	10	39
2	0.642	6	43
2	0.836	3	61
4	0.074	11	14
		22	27
4	0.273	7	42
4	0.495	6	94

TABLE 1. Parameters for simulations. Two types of numerical experiments were performed: (1) (see above) fix the size ratio of spheres, λ, at 2 or 4 and the area fraction of solids, ϕ_a, at 0.503, then vary the fraction of small spheres, ξ; (2) (not shown) set $\xi = 0.27$ and for seven values of ϕ_a (0.118, 0.236, 0.354, 0.453, 0.503, 0.55, 0.60) determine the effect of varying the size ratio of spheres from $\lambda = 1$ to $\lambda = 4$.

Ewald sum method developed by Brady *et al.* (1988) which gives rigorously convergent particle interactions by correctly describing the 'back flow' of fluid (Batchelor 1972). However, when all particles are in the same plane, such convergence difficulties are absent, and it is not necessary to explicitly take the back-flow effects into account (Bossis & Brady 1990).

In our simulations, a unit cell consisted of suspensions having 25, 49, 64, or 100 particles. The number of particles used for a simulation depends on the size ratio of the spheres and the fraction of small spheres in a suspension. We sought to make the periodic cell sufficiently large in order to reduce the $O(l^{-2})$ error term in the long-range interactions. The simulations began with the particles located at random positions in a periodic cell. Microstructural changes were calculated in time until steady state was reached. The steady state was determined by monitoring the average of the square of the x- and y-components of the particle velocities relative to the bulk shear flow. Actually, steady state is defined on a time-averaged basis, with small fluctuations occurring on short timescales. Steady state was reached in approximately twenty strain units (γ = shear rate times time). Examining the x- and y-components of the translational part of $U - U^{\infty}$, $u_x - \dot{\gamma}y$ and u_y respectively, for monodispersed suspensions, we find that $\Delta u_x^2 = (u_x - \dot{\gamma}y)^2 \approx u_y^2$ for $\phi_a \leqslant 0.45$. As ϕ_a increases from 0.45, $\Delta u_x^2 > u_y^2$, since u_x decreases due to hindered mobility caused by the presence of large particle clusters while $\dot{\gamma}y$ remains fixed and u_y increases only slightly. For bimodal suspensions, the velocities of both the large and small spheres behave similar to those in the monodispersed case. However, for dilute suspensions, we find that the total translational velocity of the small and large spheres, u_s and u_l, respectively, satisfy $u_s^2 > u_l^2$ due to the larger drag on the large spheres and the lack of large clusters. At high ϕ_a, say $\phi_a \geqslant 0.5$, we find that $u_s^2 \approx u_l^2$ since the large and small particles together form clusters which move through the fluid as a single entity.

For the simulations $\dot{\gamma} = 1$, and a time step of 2×10^{-4} was used. Hence, steady state generally occurred after 100000 time steps with the calculations being carried out to a total 200000 time steps. The pair-distribution functions, cluster size information and relative viscosities reported below were averaged over the last 100000 time steps. To determine the statistical errors, simulations under the same conditions of area fraction, size ratio, and fraction of small particles were conducted starting from five different initial conditions resulting in a total of 1000000 time steps. We report simulation

results for area fractions up to 0.6. For more concentrated systems the time step must be reduced to accurately follow the particle trajectories. Owing to computational limitations, such simulations were not conducted. All calculations were performed in double precision on either an IBM 3090, a DEC 5000/200 Workstation, or a Cray YMP. The different simulation conditions are given in table 1. This summarizes the size ratio of spheres, λ, the number of particles, N, the number of small spheres, N_s, and the number of large spheres, N_l, the fraction of total solids that were small spheres, ξ, and the fraction of total area taken by the solids, ϕ_a.

3. Results

In this section we present dynamic simulation results for both microscopic (pair-distribution function and cluster formation) and macroscopic (viscosity) properties of bimodal suspensions. Figure 3(*a*) shows a typical initial configuration of a bimodal suspension having $\phi_a = 0.503$, $\xi = 0.273$ and $\lambda = 2$. At $t = 0$, the particles are located randomly in the periodic cell by first placing the spheres in a regular array and then perturbing them a small random distance. The only constraint placed on the random displacements is that they not be so large as to cause particles to develop. The dashed line shows the boundary of the unit cell. Figure 3(*b*) depicts an instantaneous suspension microstructure after steady state was reached, that is after twenty strain units. This figure qualitatively shows that small spheres tend to fit in the spaces among the large spheres and that the particles aggregate in clusters. These clusters tend to form along the compressive flow direction ($\theta = 135°$) and rotate as a solid rod, then break up in the extensional flow direction ($\theta = 45°$). This is similar to the behaviour described by Brady & Bossis (1988) in monodispersed suspensions. This phenomenon can be easily seen by generating a series of computer animations of the particle motions. Typically, for such 'movies', we plot the instantaneous suspension microstructure for every 250 time steps and then animate them with a total of 800 frames. Such animations show qualitatively that clusters continuously form and break up as described above. These animations may be obtained from the authors.

Prior to calculating the rheology of bimodal suspensions we tested our formulae and procedures by computing the relative viscosities of monodispersed suspensions. We specialized our equations for the bimodal case to those for particles of the same size. Figure 4 compares our simulation results with experiments and with the simulation results of Brady & Bossis (1985). Consistent with the simulations, the data are for large Péclet numbers ($> 10^6$). The error bars represent the standard deviation derived from five different simulations with differing initial conditions. Following Brady & Bossis (1985), all concentrations are normalized by the two-dimensional maximum packing fraction, $\phi_m^{2d} = 0.785$, and three-dimensional maximum packing fraction, $\phi_m^{3d} = 0.605$, to allow comparison between simulation and experiment. The similarity among the three-dimensional experimental results (Rutgers 1962; Gadala-Maria 1979; Pätzold 1980), the two-dimensional simulation results of Brady & Bossis (1985) and our own work is very good. However, as noted by Brady & Bossis (1985), the ratio of the maximum packing fractions, ϕ_m^{2d} to ϕ_m^{3d}, acts as an adjustable parameter. Different values shift curves horizontally, but not significantly for reasonable choices of ϕ_m^{2d} and ϕ_m^{3d}. However, the influence is especially large for concentrations near the maximum packing.

For bimodal suspensions, the simulation results for the dependence of the relative viscosities on particle size ratio with the fraction of small spheres fixed are given in figure 5. For $\xi = 0.27$, the size ratio affects the relative viscosity, particularly for large

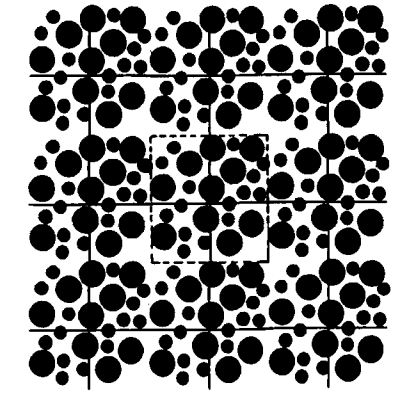

(*a*)

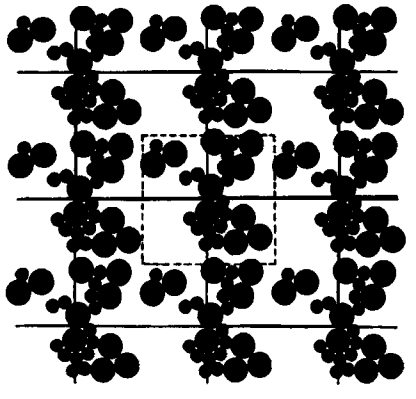

(*b*)

FIGURE 3. (*a*) Initial configuration for a randomly distributed bimodal suspension. The total area fraction is 0.503 with $\xi = 0.27$ and $\lambda = 2$. The dashed lines are the boundaries of the periodic cell. (*b*) An instantaneous suspension microstructure after steady state was reached. Small spheres tend to fit in the spaces among the large spheres and the particles form clusters.

ϕ_a. For example, if $\phi_a = 0.55$, η_r decreases as λ increases. However, the reduction in the relative viscosity of a bimodal suspension becomes significant only when $\phi_a > 0.45$. Error bars in figure 5 represent one standard deviation based upon the average relative viscosity calculated for each of the simulations once steady state was achieved. Qualitatively, the results in figure 5 show the same trend as the experimental data given in figure 1. A similar correspondence between the experiments and the simulations is given in figure 6. This depicts the dependence of the relative viscosity upon the fraction of small spheres at a fixed area fraction ($\phi_a = 0.5$). For λ fixed, say $\lambda = 2$, the relative viscosity initially decreases as ξ increases from zero. It reaches a minimum around $\xi = 0.25$ and then increases as $\xi \to 1$. Similar results are found for $\lambda = 4$, although here we only show simulation results up to $\xi = 0.5$. This limitation results from the requirements that the size of the periodic cell be large enough to minimize the $O(l^{-2})$ errors caused by the particles outside the periodic cell, as mentioned in §2. To achieve this, over 150 particles would be needed to accurately simulate a suspension having $\phi_a = 0.5$, $\xi > 0.5$ and $\lambda = 4$. Although dynamic simulations with 150 particles per unit

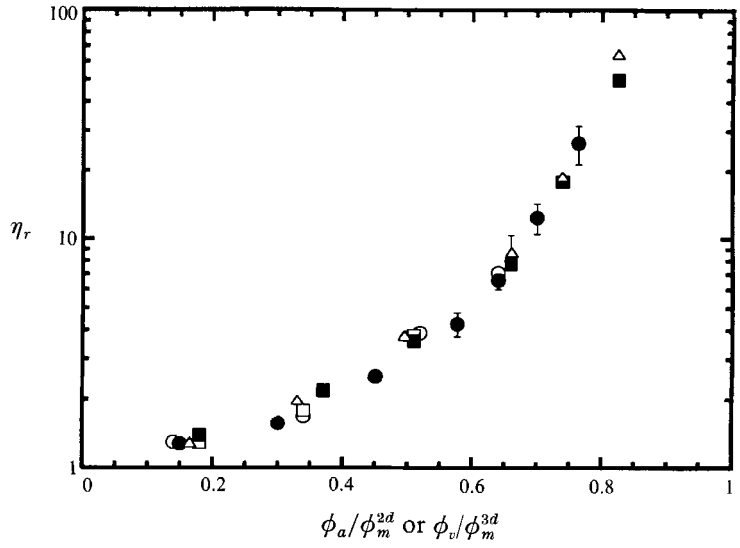

FIGURE 4. Comparison of the simulation of monodispersed viscosities with experiment and with the simulation results of Brady & Bossis (1985). As in Brady & Bossis, all concentrations have been normalized by the maximum packing fraction, $\phi_m^{2d} = 0.785$ and $\phi_m^{3d} = 0.605$, to compare two- and three-dimensional results. The error bars indicate experiment errors and the statistical uncertainties in simulations. ○, Brady & Bossis 1985; □, Gadala-Maria (1979); ■, Pätzold (1980); △, Rutgers (1962); ●, present work.

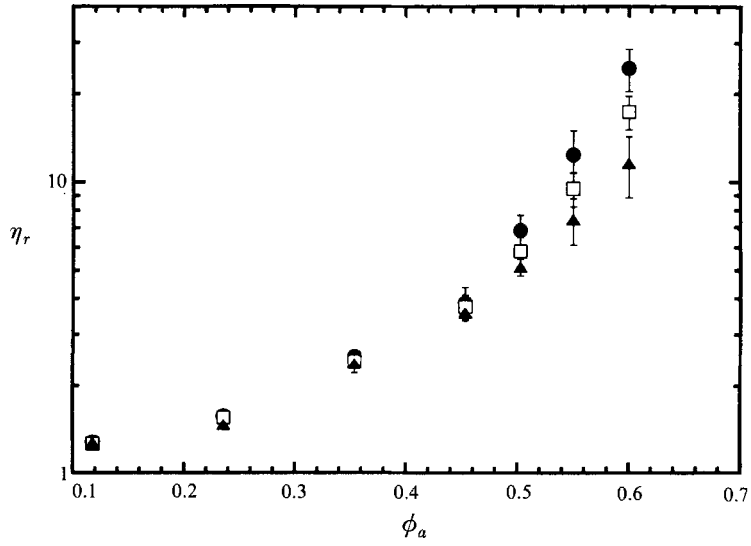

FIGURE 5. Dependence of the relative viscosities, η_r, on particle size ratio, λ, with fraction of small spheres fixed at $\xi = 0.27$: ●, monodispersed, $\lambda = 1$; □, $\lambda = 2$; ▲, $\lambda = 4$.

cell are possible with current workstations, it might take over one week with a dedicated unit to actually do the calculations. It is possible to reduce the total number of particles and avoid the $O(l^{-2})$ errors by using the Ewald summation technique (Brady *et al.* 1988; Brady & Bossis 1988). The hydrodynamic mobility and resistance matrices that result from this technique correctly include all far-field non-convergent interactions. However, even with the Ewald summation technique, many more

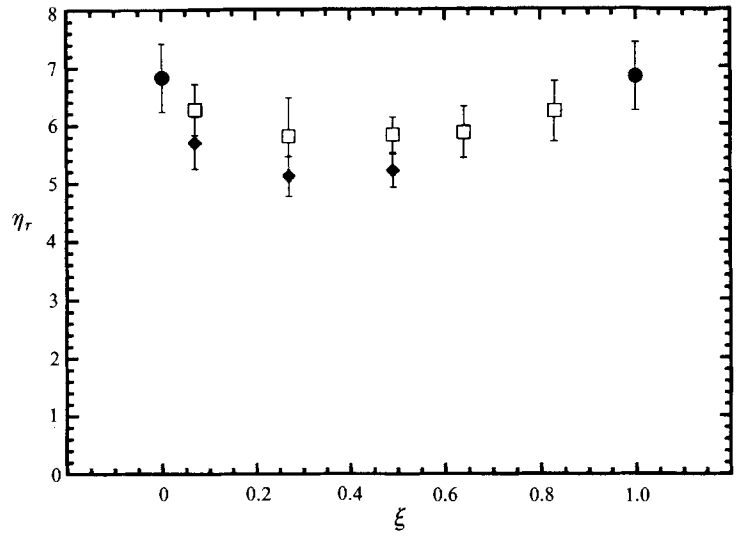

FIGURE 6. Dependence of the relative viscosities, η_r, on the fraction of small spheres, ξ, with area fraction, ϕ_a, fixed at 0.5: ●, monodispersed, $\lambda = 1$; □, $\lambda = 2$; ◆, $\lambda = 4$.

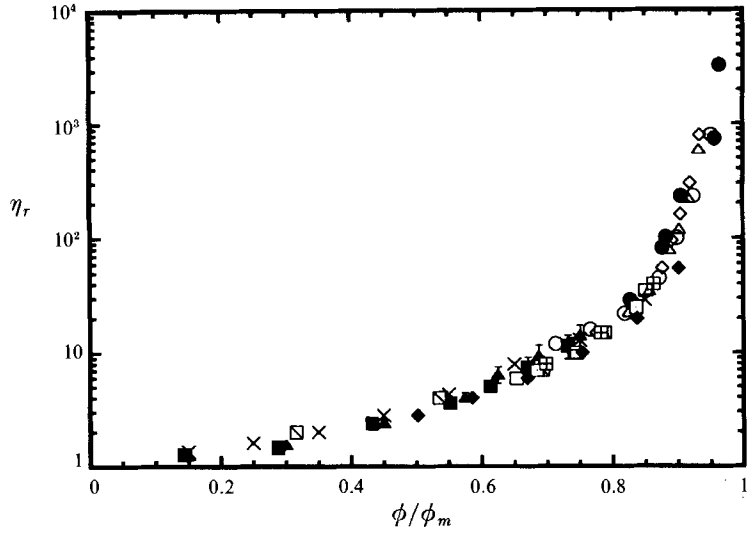

FIGURE 7. Comparison of the relative viscosities of bimodal suspensions obtained by simulations with experiment. All area and volume fractions have been normalized by the maximum packing fractions given in table 2, where the symbols used are also defined. The error bars for the simulation results represent one standard deviation.

particles than we are currently using would be required to greatly extend the range of parameters in simulations of bimodal suspensions. For example, for a suspension having $\phi_a = 0.55$, $\lambda = 8$ and $\xi = 0.8$, at least 256 small particles and one large particle are needed.

A comparison of the results for the two-dimensional simulations with experiments can only be undertaken if we account for the difference in the maximum packing between the two- and three-dimensional cases (Brady & Bossis 1985). For example, for monodispersed suspensions, maximum close packing for a three-dimensional lattice is

Reference	λ	ξ	ϕ_m^{3d} or ϕ_m^{2d}		Symbols (figure 7)
Chong *et al.* (1971)	2	0.25	0.654	—	△
	3.2	0.25	0.696	—	◇
	7.2	0.25	0.757	—	○
Poslinski *et al.* (1988)	5.2	0.30	0.74	—	×
	5.2	0.50	0.72	—	×
Storms *et al.* (1990)	2.31	0.5	0.635	—	⊠
	2.96	0.5	0.657	—	⊡
	4.1	0.5	0.684	—	⊞
	4.93	0.5	0.696	—	□
Shapiro & Probstein (1992)	4	0.5	0.597	—	◆
Present work	2	0.27	—	0.8	▲
	4	0.27	—	0.82	■
Chang (1992)	2.5	0.25	0.701	—	●
(Experiment)	7.5	0.25	0.76	—	●
	13.75	0.25	0.81	—	●
	2.5	0.5	0.695	—	●
	7.5	0.5	0.74	—	●
	13.75	0.5	0.77	—	●

TABLE 2. Values of ϕ_m^{3d} and ϕ_m^{2d} for bimodal suspensions.

0.74 whereas in two-dimensions an area loading up to 0.9 can be achieved. In the case of the simulations presented in figure 4, we used values suggested by Brady & Bossis (1985) to normalize ϕ_a and ϕ_v. For bimodal suspensions, values of ϕ_m^{3d} are available in the literature (Chong *et al.* 1971; Poslinski *et al.* 1988). These values are generally determined experimentally. The two-dimensional close-packing values can be found in the work of Kauseh, Fesko & Tschoegl (1971) who determined the maximum packing fractions for randomly distributed bimodal distributions of circles in a plane. The results from these studies for both the two- and three-dimensional cases are generally consistent with other work (McGeary 1961; Lee 1970; Patton 1979; Visscher & Bolsterli 1972).

Figure 7 shows the comparison between the simulation results for the relative viscosity and experimental results in terms of ϕ_a/ϕ_m^{2d} and ϕ_v/ϕ_m^{3d}. The actual maximum-packing values used in obtaining the curve in figure 7 are given in table 2. In the case of the experimental data, the values which are used are those given by the investigators. In normalizing the simulation results, we have estimated ϕ_m^{2d} using the work of Kauseh *et al.* (1971). The agreement between the simulation and experimental results in figure 7 is remarkable. All of the dependence of the relative viscosity upon λ and ξ is through the dependence of the maximum packing fraction upon these geometrical parameters. Hence, if the information on the maximum packing as functions of λ and ξ (Storms *et al.* 1990; Shapiro & Probstein 1992) is coupled with the master curve in figure 7, the relative viscosity of a bimodal suspension can be determined. Although the simulation results are only for values of ϕ_a/ϕ_m^{2d} up to 0.75, the calculation of the relative viscosities for higher solid concentrations is feasible. However as the concentration increases, numerical errors can cause particles to overlap in going from one time step to the next. This can be overcome by reducing the time step, which might be very costly.

We now turn our attention to the microstructure of the suspensions to ascertain the connection between the reduction in the relative viscosity for bimodal suspensions and

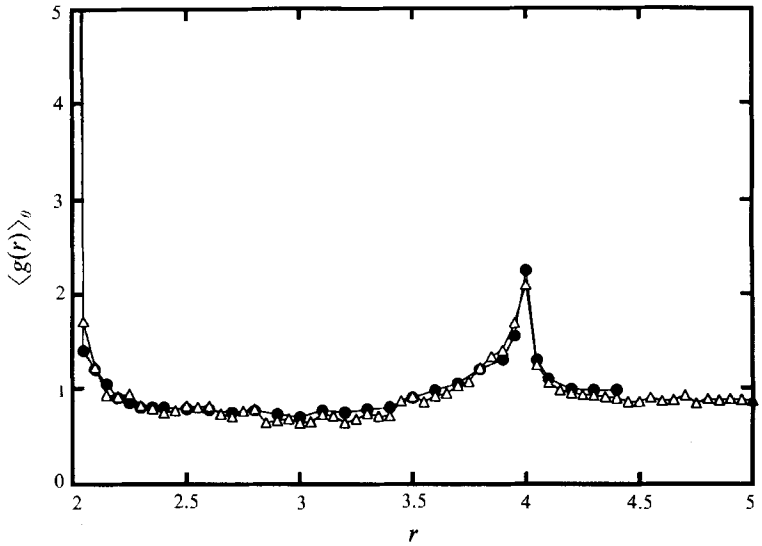

FIGURE 8. Comparison of the radial dependence of the angle-averaged pair-distribution function $\langle g(r)\rangle_\theta$ with data from Brady & Bossis (1988) at $\phi_a = 0.4$ for monodispersed suspensions. To obtain $\langle g(r)\rangle_\theta$, a simple θ-average was used with four values of θ: 9°, 27°, 99°, and 171°. The dimensionless sphere diameter is 2. △, Present work; ●, Brady & Bossis (1988).

the microrheological properties. The pair-distribution function, $g(r,\theta)$, is frequently used as a fundamental measure of the microstructure (Reed & Gubbins 1973; Bossis & Brady 1984). This is defined as the probability of finding a particle centre at r and θ relative to a particle located at $r = 0$, divided by the number density. To calculate $g(r,\theta)$ for our two-dimensional simulations, we examine the region $\theta-\Delta\theta$ to $\theta+\Delta\theta$ and $r-\Delta r$ to $r+\Delta r$. Here, the number of particles with centres in the region is found and divided by the area of the region times the number density to obtain $g(r,\theta)$. This process is repeated for various values of r and θ to determine both the angular and radial structure of the suspension. The number density is simply N/A, where N is the total number of spheres and A is the area of the periodic cell.

Initial results for $g(r,\theta)$ were obtained for monodispersed suspensions having $\phi_a = 0.4$ and compared with the results given by Brady & Bossis (1988). This comparison is shown in figure 8 in terms of $\langle g(r)\rangle_\theta$, which is a simple θ-average, using four different angles: 9°, 27°, 99°, and 171° (Bossis & Brady 1984). The excellent agreement further validates our simulation methodology. Figure 8 shows that a sphere of dimensionless diameter two is most likely to find a nearly touching neighbour. There is some likelihood, although much lower, of finding a sphere at $r = 4$, indicating the formation of linear chains of particles.

Figure 9 presents two sets of $\langle g(r)\rangle_\theta$ for bimodal suspensions with $\phi_a = 0.50$ and $\xi = 0.27$ in both cases but for different size ratios, $\lambda = 2$ and 4. Figure 9(*a*) demonstrates that for a size ratio of 2 the large spheres have higher probabilities of finding small spheres as nearest neighbours (the first peak) than large spheres (the second peak). Some small–large and small–small sphere doublets are also formed adjoining the reference large particle. For example, near a large sphere, there is a high probability of finding a small sphere at $r = 3$ and a large sphere at $r = 6$ (small–large doublet). Figure 9(*b*), which shows $\langle g(r)\rangle_\theta$ for the small spheres in a $\lambda = 2$ suspension, demonstrates that a small sphere has a higher probability of finding a large sphere as its nearest neighbour (the second peak) rather than another small sphere (the first peak). Figures

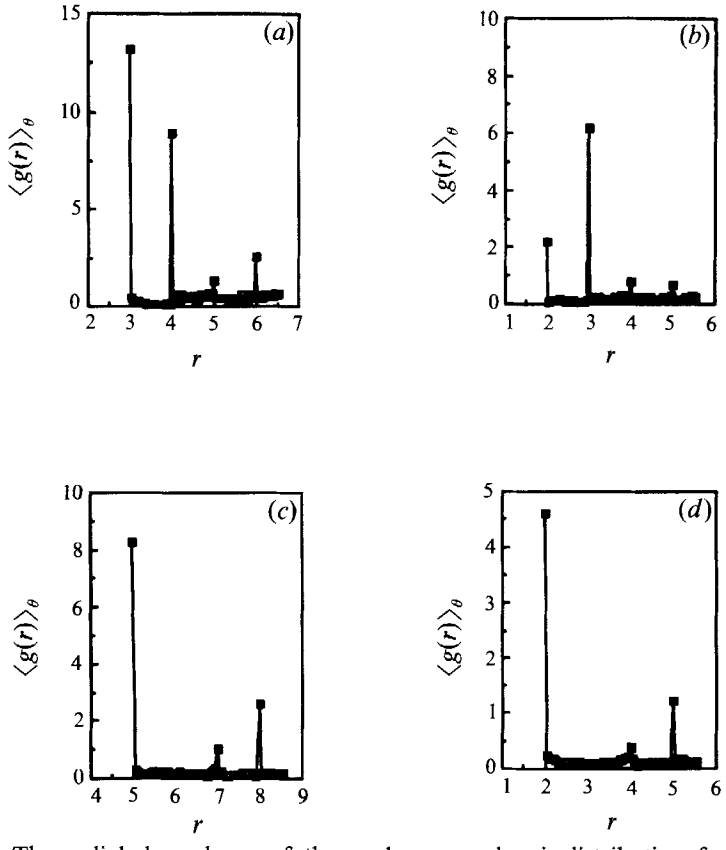

FIGURE 9. The radial dependence of the angle-averaged pair-distribution function, $\langle g(r)\rangle_\theta$ for bimodal suspensions having $\phi_a = 0.50$ and $\xi = 0.27$. (*a*) $\langle g(r)\rangle_\theta$ relative to a large sphere for $\lambda = 2$; (*b*) $\langle g(r)\rangle_\theta$ relative to a small sphere for $\lambda = 2$; (*c*) $\langle g(r)\rangle_\theta$ relative to a large sphere for $\lambda = 4$; (*d*) $\langle g(r)\rangle_\theta$ relative to a small sphere for $\lambda = 4$.

9(*c*) and 9(*d*) both show similar data for a suspension in which $\lambda = 4$. Here large and small spheres are found to have higher probabilities of finding small spheres as their nearest neighbours (the first peaks). Since there are many more small spheres than large spheres (see table 1) this might be expected. It is worth noting, however, that after large–small and small–small pairs, the next highest probabilities fall to large–large and small–large pairs. From all of the data in figure 9 one can conclude that the particle pairs (large–large, large–small, or small–small spheres) are essentially 'touching', separated only by lubrication forces. Further, three or more spheres generally form linear chains.

The pair-distribution function offers one measure of the microstructure of suspensions, but it is neither the only nor necessarily the most important one. Brady & Bossis (1988) have found that the formation of larger aggregates or clusters of particles is far more important in determining the macroscopic properties of suspensions. In monodispersed suspensions, the presence of large clusters can be directly linked to high viscosities (Brady & Bossis 1988; Bossis & Brady 1989). Further, Bossis, Meunier & Brady (1991) found that for fractal aggregates of force-free particles held together by hydrodynamic lubrication forces, the stress grows as the number of particles in the aggregates rather than as the cube of the radius of gyration. Although not a system of fractal aggregates, we hypothesized that the reduction of the relative

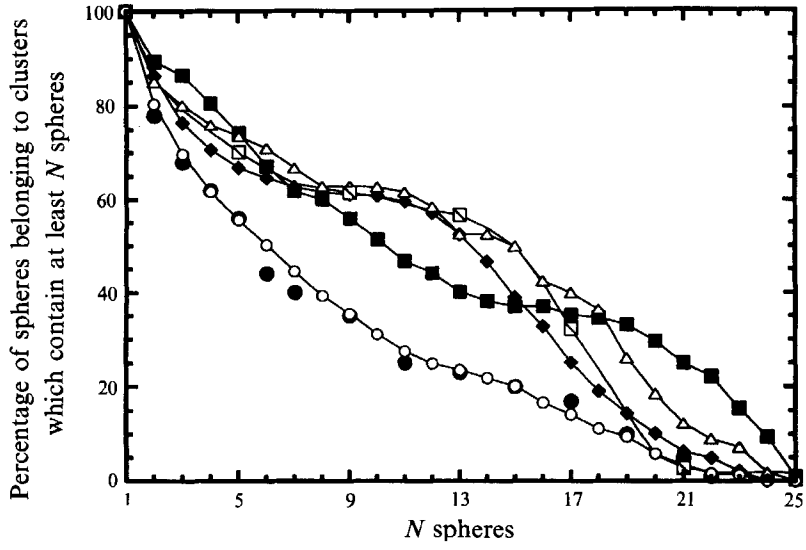

FIGURE 10. Distribution of particle cluster sizes for suspensions of spheres. For monodispersed suspensions, as the concentration is increased the cluster sizes increase. At a fixed concentration, the presence of small particles decreases the cluster sizes. ●, Bossis & Brady (1989) $\lambda = 1$, $\phi_a = 0.45$; present study: ○, $\lambda = 1$, $\phi_a = 0.45$; ■, $\lambda = 1$, $\phi_a = 0.5$; △, $\phi_a = 0.5$, $\lambda = 2$, $\xi = 0.07$; ⧅, $\phi_a = 0.5$, $\lambda = 4$, $\xi = 0.07$; ◆, $\phi_a = 0.5$, $\lambda = 2$, $\xi = 0.25$.

viscosities for bimodal suspensions as compared with monodispersed suspensions is also related to the influence of cluster size in the suspensions. Figure 10 shows the distribution of cluster sizes in monodispersed suspensions and in bimodal suspensions for various values of λ and ξ. This figure presents the percentage of spheres belonging to clusters which contain at least N spheres as a function of the size (in terms of the number of spheres) of each cluster. Following Bossis & Brady (1989), we have chosen the non-dimensionalized length as 10^{-2} for the separation distance which defines that two spheres belong to the same cluster. We first compared our results for monodispersed suspensions with the results of Bossis & Brady (1989) for $\phi_a = 0.45$ and found good agreement. To establish a baseline for bimodal suspensions, we performed a similar analysis at $\phi_a = 0.5$ for a monodispersed suspension. Then calculations were undertaken for a series of bimodal suspensions. As figure 10 shows, the monodispersed suspension has a higher percentage of spheres belonging to large clusters than bimodal suspensions. Comparing the bimodal suspensions, we see that a suspension having $\lambda = 2$ and $\xi = 0.07$ has a higher percentage of spheres belonging to large clusters than either a suspension having $\lambda = 2$ and $\xi = 0.27$ or $\lambda = 4$ and $\xi = 0.07$. This indicates that the presence of smaller particles tends to reduce average cluster size in a suspension and hence correlates with the dependence of the relative viscosity of bimodal suspensions upon λ and ξ, as shown in figures 5 and 6.

Figure 11 shows the comparison of the ratio of the number of small spheres to the number of large spheres in clusters as a function of the ratio of the number of small spheres to the number of large spheres in the overall suspension. These data are for $\phi_a = 0.50$ and include all size ratios and all values of ξ used in the simulations. Two sizes of clusters were considered: those having 10 and 20 particles. The particle size distribution in the clusters is approximately linear with respect to the overall size distribution. Hence, there is no preference for particles of a particular size to form clusters and effect size segregation during simple shear.

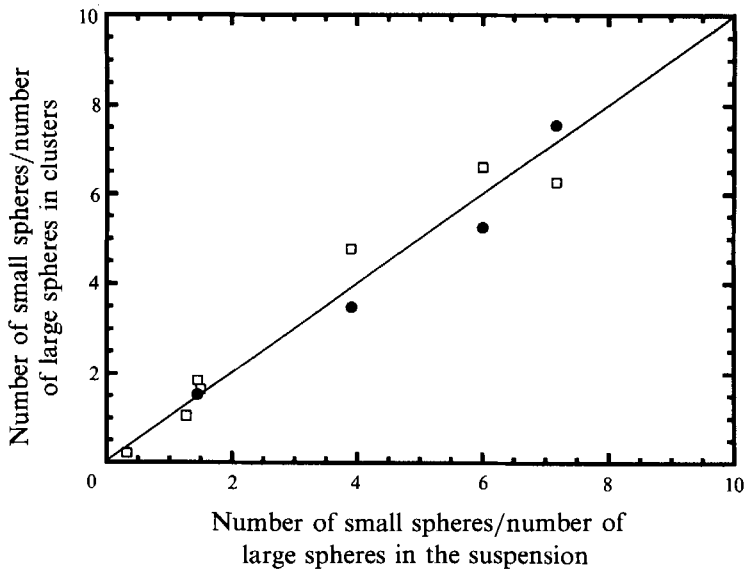

FIGURE 11. The ratio of the number of small spheres to that of large spheres in clusters versus the ratio of the number of small spheres to that of large spheres in the overall suspension: □, cluster size of 10 spheres; ●, cluster size of 20 spheres.

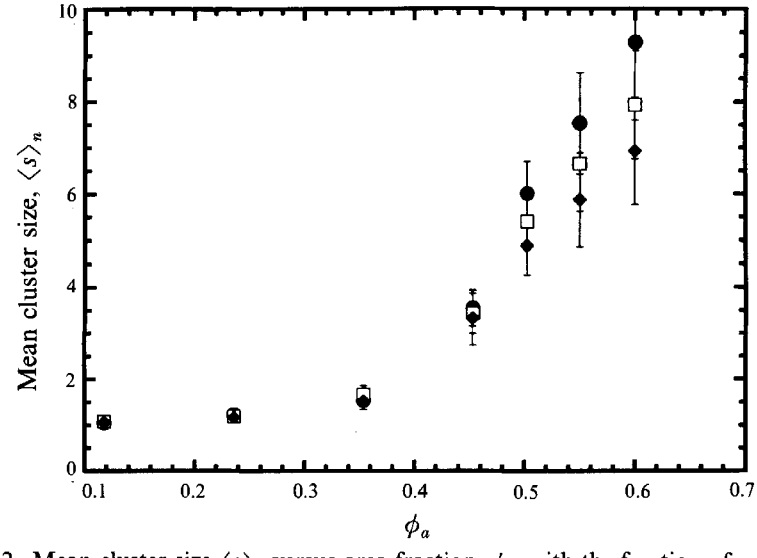

FIGURE 12. Mean cluster size $\langle s \rangle_n$ versus area fraction, ϕ_a, with the fraction of small spheres fixed at 0.27: ●, monodispersed, $\lambda = 1$; □, $\lambda = 2$; ◆, $\lambda = 4$. The trend shown here is similar to that found for the relative viscosity, see figure 5.

The cluster size distribution can also be measured through the number-averaged mean cluster size

$$\langle s \rangle_n = \sum_s s n_s / \sum_s n_s, \tag{3.1}$$

where n_s is the number of clusters containing s spheres. For a fixed fraction of small particles, $\xi = 0.27$, figure 12 shows that at high concentrations (say, $\phi_a > 0.5$) the mean cluster size $\langle s \rangle_n$ decreases as the size ratio of spheres increases. This is exactly the same trend as found for the viscosity, as shown in figure 5. The similarity between the

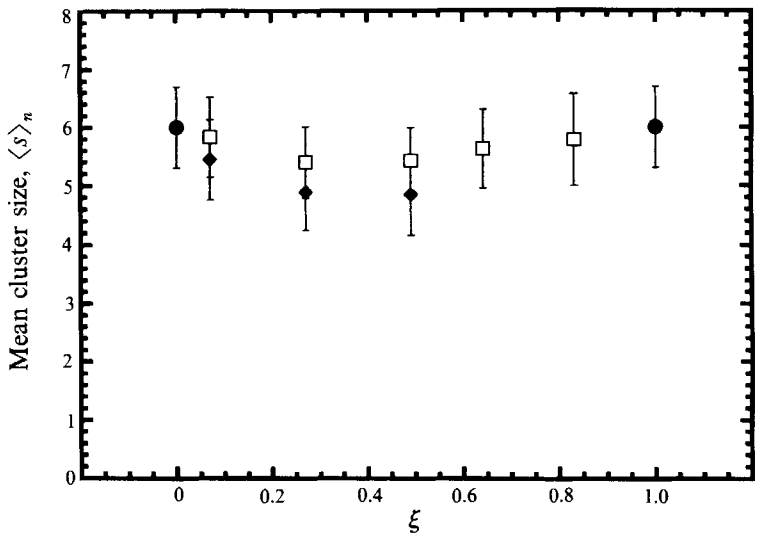

FIGURE 13. Mean cluster size $\langle s \rangle_n$ versus the fraction of small spheres, ξ, at a constant area fraction, $\phi_a = 0.5$: ●, monodispersed, $\lambda = 1$; □, $\lambda = 2$; ◆, $\lambda = 4$. The trend show here is similar to that found for the relative viscosity, see figure 6.

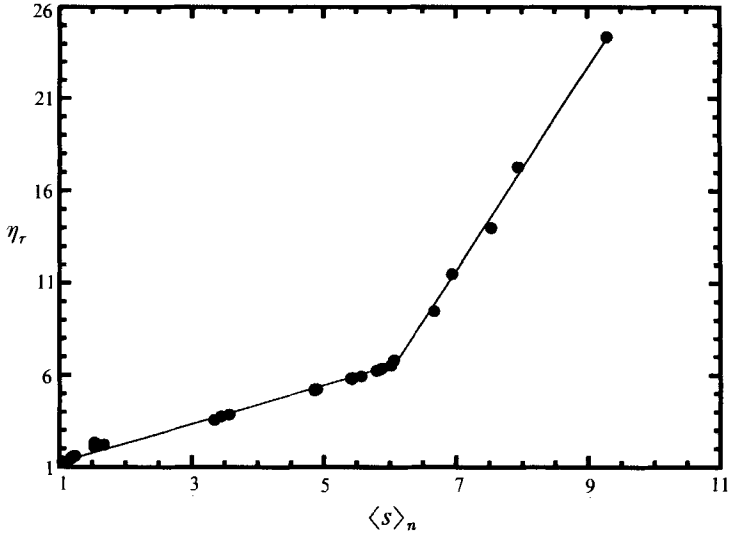

FIGURE 14. Dependence of the relative viscosity, η_r, upon the mean cluster size, $\langle s \rangle_n$. Values of the area fraction, ϕ_a, range from 0.12 to 0.60 with $\xi = 0.27$ and $\lambda = 1$, 2 and 4; and at $\phi_a = 0.50$, ξ ranges from 0.073 to 0.836 for $\lambda = 1$, 2 and 4.

behaviour of η_r and $\langle s \rangle_n$ is further seen in figure 13 where the relationship between $\langle s \rangle_n$ and the fraction of small spheres at a fixed area fraction, $\phi_a = 0.5$, is shown. For a fixed size ratio, e.g. $\lambda = 2$, $\langle s \rangle_n$ decreases as ξ increases from zero. After reaching a minimum value, the viscosity increases as $\xi \rightarrow 1$. Again, this is the same trend as that found for the viscosity, as shown in figure 6.

By combining the dependencies of η_r and $\langle s \rangle_n$ upon λ and ξ, given in figures 5, 6, 12 and 13, we can determine the relationship between η_r and $\langle s \rangle_n$, which is given in figure 14. The relative viscosity scales linearly with $\langle s \rangle_n$ for both small and large mean cluster sizes, but there is a distinct break in the actual linear form around $\langle s \rangle_n = 6$.

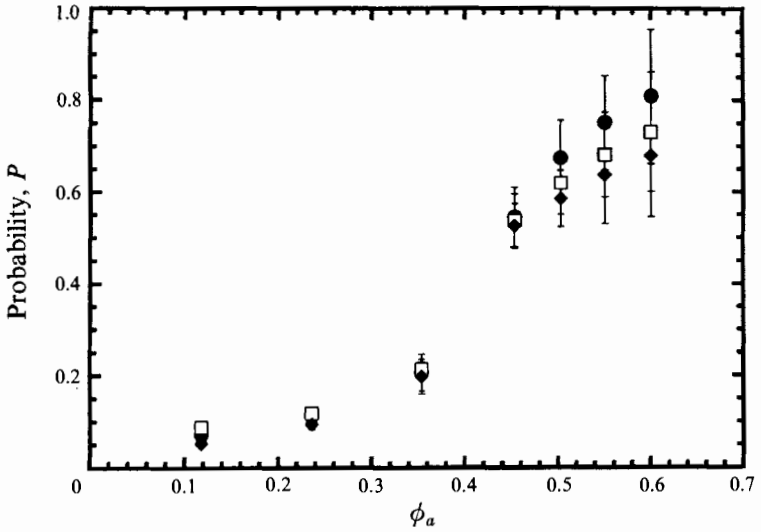

FIGURE 15. Probability, P, versus area fraction, with the fraction of small spheres fixed at 0.27: ●, monodispersed, $\lambda = 1$; □, $\lambda = 2$; ◆, $\lambda = 4$. The trend shown here is similar to that found for the relative viscosity, see figure 5.

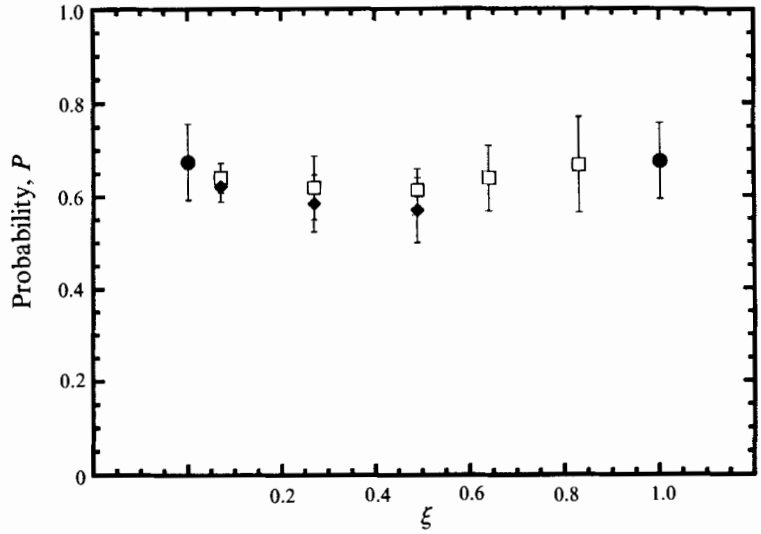

FIGURE 16. Probability, P, versus the fraction of small spheres, with the area fraction of solids fixed at 0.5: ●, monodispersed, $\lambda = 1$; □, $\lambda = 2$; ◆, $\lambda = 4$. The trend shown here is similar to that found for the relative viscosity, see figure 6.

When $\phi_a \ll 1$, that is $\langle s \rangle_n \to 1$, η_r tends towards 1 with the actual least-squares fit providing $\eta_r = 1.06\langle s \rangle_n + 0.067$, for $\langle s \rangle_n \leqslant 6$. For $\langle s \rangle_n > 6$, $\eta_r = 5.46\langle s \rangle_n - 26.3$. Since the conditions that provide $\langle s \rangle_n > 6$ appear at $\phi_a \geqslant 0.5$ for $\lambda = 1$, $\phi_a \geqslant 0.55$ for $\lambda = 2$ and $\phi_a \geqslant 0.6$ for $\lambda = 4$ (see figure 12), we believe that the transition point corresponds to the onset of percolation. It is possible that large clusters bridge the periodic cell in such concentrated suspensions. Indeed, if we determine the size of the largest cluster in our suspensions, we find that for $\lambda = 1$, 2 and 4, the largest cluster

spans the unit cell for $\phi_a \geqslant 0.5$, 0.55 and 0.6, respectively. Experimentally, one would also expect percolation to occur in highly concentrated suspensions undergoing simple shear (except in the depletion layer near the walls) due to the hydrodynamic lubrication forces between particles in the clusters.

Another measure of cluster formation is the probability $P = N^+/N$, where N^+ is the number of spheres which belong to the biggest cluster and N is the total number of spheres in the simulation. In figure 15 we show that at high concentration (say $\phi_a = 0.50$) with ξ fixed at 0.27, the probability P decreases as the size ratio of spheres increases. Again, these curves show the same trend as the viscosity curves shown in figure 5. In figure 16, we see that as size ratio of spheres is fixed (say $\lambda = 2$) and the area fraction of solids is also fixed at 0.50, the probability P has the same trend with ξ as the viscosity curve shown in figure 6. Again, this demonstrates that the reduction of relative viscosities in bimodal suspensions is linked to the reduction of cluster size in the suspensions.

4. Conclusions

In this paper we have shown that Stokesian dynamics can be extended to compute both microstructural dynamics and macroscopic rheological properties of bimodal suspensions of hydrodynamically interacting spherical particles. At the microstructural level, we determined the pair-distribution functions and cluster formation; the macroscopic property was the relative viscosity. The method we described in §2 captures the essential physics of the hydrodynamic interactions in a suspension of unequal-sized spheres. Both the dominant far-field many-body interactions and the near-field lubrication forces are explicitly included. We have used periodic boundary conditions to represent an infinite suspension. All of our simulations used a monolayer of spheres to minimize the computation costs while preserving the physics in the plane of shear. The good agreement between simulations and experiments for the relative viscosity indicate that Stokesian dynamics is capable of excellent quantitative predictive ability for bimodally distributed suspensions of spheres of varying volume fraction and size ratio. It also provides definitive evidence that the maximum packing fraction appropriately scales the overall volume fraction so as to collapse the relative viscosity dependency upon the normalized volume fraction to a single master curve for bimodal suspension.

Cluster formation, a direct result of the hydrodynamic lubrication forces that keep particle surfaces from touching, correlates with the lower viscosity measured for bimodal suspensions relative to a monodispersed suspension at the same particle loading. The results in §3 show that the viscosity reduction for bimodal suspensions is directly linked to the influence of particle size distribution on the average cluster size in a suspension.

We have only considered hydrodynamic interactions among particles, but the extension to include interparticle forces and Brownian motion is straightforward (Bossis & Brady 1984, 1987, 1989; Brady & Bossis 1985; Bossis, Brady & Mathis 1988). For colloidal dispersions of unequal-sized spherical particles, in addition to ϕ_a (or ϕ_v), λ and ξ, the absolute size of the particles also plays an important role in determining the flow behaviour of the suspensions (Sengun & Probstein 1989*a*, *b*; Hoffman 1992). In particular, the data of Hoffman (1992) suggest that the effects of both λ and ξ can be dominated by effects due to the absolute particle size. Future work will be aimed at including the effects of interparticle and Brownian forces for bimodal suspensions. We also expect, either by increasing our computational resources or developing algorithms

utilizing the Ewald summation technique, to extend our results to larger size ratios, such as $\lambda = 8$, which will allow the smaller spheres to fit among the larger ones more easily.

This work was supported by the Chemical Systems Division (CSD) of United Technologies through the efforts of Dr R. R. Miller. The authors wish to thank Professor John Brady for his help in initiating this study. Professors David Jeffrey and Sangtae Kim graciously allowed us to see early versions of manuscripts that also became central to our research.

Appendix: Elements of the grand mobility matrix for unequal-sized (bimodal) spheres

The grand mobility matrix $\boldsymbol{M}^{\infty}$ in (2.4) written in terms of identical elements using the notation of Durlofsky *et al.* (1987) (also Jeffrey & Onishi 1984 and Jeffrey 1992) and of this paper. We non-dimensionalized all lengths by a characteristic length $\boldsymbol{e}$, and the individual matrices $\boldsymbol{a}$, $\boldsymbol{b}$, etc. by $6\pi\mu e^n$, where $n = 1$ for $\boldsymbol{a}$, 2 for $\boldsymbol{b}$ and $\boldsymbol{g}$, and 3 for the remaining elements. We now proceed to write the elements of $\boldsymbol{M}^{\infty}$. Letting r denote the centre–to-centre separation of spheres α and β and $e_i = r_i/r$, the unit vector joining α to β, the symmetry of the two-sphere geometry enables us to write

$$
\begin{aligned}
a_{ij}^{\alpha\beta} &= x_{\alpha\beta}^{a} e_i e_j + y_{\alpha\beta}^{a}(\delta_{ij} - e_i e_j),\\
b_{ij}^{\alpha\beta} &= y_{\alpha\beta}^{b} \epsilon_{ijk} e_k,\\
c_{ij}^{\alpha\beta} &= x_{\alpha\beta}^{c} e_i e_j + y_{\alpha\beta}^{c}(\delta_{ij} - e_i e_j),\\
g_{ijk}^{\alpha\beta} &= x_{\alpha\beta}^{g}(e_i e_j - \tfrac{1}{3}\delta_{ij})\, e_k + y_{\alpha\beta}^{g}(e_i \delta_{jk} + e_j \delta_{ik} - 2e_i e_j e_k),\\
h_{ijk}^{\alpha\beta} &= y_{\alpha\beta}^{h}(e_i \epsilon_{jkl} e_l + e_j \epsilon_{ikl} e_l),\\
m_{ijkl}^{\alpha\beta} &= \tfrac{3}{2} x_{\alpha\beta}^{m}(e_i e_j - \tfrac{1}{3}\delta_{ij})(e_k e_l - \tfrac{1}{3}\delta_{kl})\\
&\quad + \tfrac{1}{2} y_{\alpha\beta}^{m}(e_i \delta_{jl} e_k + e_j \delta_{il} e_k + e_i \delta_{jk} e_l + e_j \delta_{ik} e_l - 4e_i e_j e_k e_l)\\
&\quad + \tfrac{1}{2} z_{\alpha\beta}^{m}(\delta_{ik}\delta_{jl} + \delta_{jk}\delta_{il} - \delta_{ij}\delta_{kl} + e_i e_j \delta_{kl} + \delta_{ij} e_k e_l\\
&\quad + e_i e_j e_k e_l - e_i \delta_{jl} e_k - e_j \delta_{il} e_k - e_i \delta_{jk} e_l - e_j \delta_{ik} e_l).
\end{aligned}
$$

Consistent with the approximation in (2.11) and (2.15), (2.16), the scalar mobility functions are

$$
\begin{aligned}
&x_{11}^{a} = y_{11}^{a} = e/a, \quad x_{12}^{a} = x_{21}^{a} = \tfrac{3}{2}e/r - \tfrac{1}{2}(a^2+b^2)\, e/r^3,\\
&x_{22}^{a} = y_{22}^{a} = e/b, \quad y_{12}^{a} = y_{21}^{a} = \tfrac{3}{4}e/r + \tfrac{1}{4}(a^2+b^2)\, e/r^3,\\
&y_{11}^{b} = -y_{22}^{b} = 0, \quad y_{12}^{b} = -y_{21}^{b} = -\tfrac{3}{4}e^2/r^2,\\
&x_{11}^{c} = y_{11}^{c} = \tfrac{3}{4}e^3/a^3, \quad x_{12}^{c} = x_{21}^{c} = \tfrac{3}{4}e^3/r^3,\\
&x_{22}^{c} = y_{22}^{c} = \tfrac{3}{4}e^3/b^3, \quad y_{12}^{c} = y_{21}^{c} = -\tfrac{3}{8}e^3/r^3,\\
&x_{11}^{g} = -x_{22}^{g} = 0, \quad y_{11}^{g} = -y_{22}^{g} = 0,\\
&x_{12}^{g} = \tfrac{9}{4}e^2/r^2 - \tfrac{9}{4}b^2e^2/r^4 - \tfrac{27}{20}a^2e^2/r^4, \quad x_{21}^{g} = -\tfrac{9}{4}e^2/r^2 + \tfrac{9}{4}a^2e^2/r^4 + \tfrac{27}{20}b^2e^2/r^4,\\
&y_{12}^{g} = \tfrac{3}{4}b^2e^2/r^4 + \tfrac{9}{20}a^2e^2/r^4, \quad y_{21}^{g} = -\tfrac{3}{4}a^2e^2/r^4 - \tfrac{9}{20}b^2e^2/r^4,\\
&y_{11}^{h} = y_{22}^{h} = 0, \quad y_{12}^{h} = y_{21}^{h} = -\tfrac{9}{8}e^3/r^3,\\
&x_{11}^{m} = y_{11}^{m} = z_{11}^{m} = \tfrac{9}{10}e^3/a^3, \quad x_{22}^{m} = y_{22}^{m} = z_{22}^{m} = \tfrac{9}{10}e^3/b^3,\\
&x_{12}^{m} = x_{21}^{m} = -\tfrac{9}{2}e^3/r^3 + \tfrac{27}{5}(a^2+b^2)\, e^3/r^5, \quad y_{12}^{m} = y_{21}^{m} = \tfrac{9}{4}e^3/r^3 - \tfrac{18}{5}(a^2+b^2)\, e^3/r^5,\\
&z_{12}^{m} = z_{21}^{m} = \tfrac{9}{10}(a^2+b^2)\, e^3/r^5.
\end{aligned}
$$

The corresponding lubrication formulae are written by defining

$$d = r - a - b/\tfrac{1}{2}(a+b) = s - 2, \quad \lambda = b/a$$

and can be found in Jeffrey & Onishi (1984), Kim & Karrila (1991) and Jeffrey (1992).

REFERENCES

BARNES, H. A., EDWARDS, M. F. & WOODCOCK, L. V. 1987 Applications of computer simulations to dense suspension rheology. *Chem. Engng Sci.* **42**, 591–608.

BATCHELOR, G. K. 1970 The stress system in a suspension of force-free particles. *J. Fluid Mech.* **41**, 545–570.

BATCHELOR, G. K. 1972 Sedimentation in a dilute dispersion of spheres. *J. Fluid Mech.* **52**, 245–268.

BATCHELOR, G. K. 1977 The effect of Brownian motion on the bulk stress in a suspension of spherical particles. *J. Fluid Mech.* **83**, 97–117.

BATCHELOR, G. K. & GREEN, J. T. 1972 The hydrodynamic interaction of two small freely-moving spheres in a linear flow field. *J. Fluid Mech.* **56**, 375–400.

BOSSIS, G. & BRADY, J. F. 1984 Dynamic simulation of sheared suspensions. I. General method. *J. Chem. Phys.* **80**, 5141–5154.

BOSSIS, G. & BRADY, J. F. 1987 Self-diffusion of Brownian particles in concentrated suspensions under shear. *J. Chem. Phys.* **87**, 5437–5448.

BOSSIS, G. & BRADY, J. F. 1989 The rheology of Brownian suspensions. *J. Chem. Phys.* **91**, 1866–1874.

BOSSIS, G. & BRADY, J. F. 1990 Diffusion and rheology in concentrated suspensions by Stokesian dynamics. In *Hydrodynamics of Dispersed Media* (ed. J.-P. Hulin, A. M. Cazabat, E. Guyon & F. Carmona). Elsevier.

BOSSIS, G., BRADY, J. F. & MATHIS, C. 1988 Shear-induced structured in colloidal suspensions. 1. Numerical simulation. *J. Colloid Interface Sci.* **126**, 1–15.

BOSSIS, G., MEUNIER, A. & BRADY, J. F. 1991 Hydrodynamic stress on fractal aggregates of spheres. *J. Chem. Phys.* **94**, 5064–5070.

BRADY, J. F. & BOSSIS, G. 1985 The rheology of concentrated suspensions of spheres in simple shear flow by numerical simulation. *J. Fluid Mech.* **155**, 105–129.

BRADY, J. F. & BOSSIS, G. 1988 Stokesian dynamics. *Ann. Rev. Fluid Mech.* **20**, 111–157.

BRADY, J. F., PHILLIPS, R. J., LESTER, J. C. & BOSSIS, G. 1988 Dynamic simulation of hydrodynamically interacting suspensions. *J. Fluid Mech.* **195**, 257–280.

CARNAHAN, B., LUTHER, H. A. & WILKES, J. O. 1969 *Applied Numerical Methods.* John Wiley & Sons.

CHAN, D. & POWELL, R. L. 1984 Rheology of suspensions of spherical particles. *J. Non-Newtonian Fluid Mech.* **15**, 165–179.

CHANG, C. 1992 The rheology of bimodal suspensions of hydrodynamically interacting spherical particles. PhD thesis, University of California at Davis.

CHENG, D. C.-H., KRUSZEWSKI, A. P., SENIOR, J. R. & ROBERTS, T. A. 1990 The effect of particle size distribution on the rheology of an industrial suspensions. *J. Materials Sci.* **25**, 353–373.

CHONG, J. S., CHRISTIANSEN, E. B. & BAER, A. D. 1971 Rheology of concentrated suspensions. *J. Appl. Polymer. Sci.* **15**, 2007–2021.

CHWANG, A. T. & WU, Y. T. 1975 Hydromechanics of low-Reynolds-number flow. Part 2. Singularity method for Stokes flows. *J. Fluid Mech.* **67**, 787–815.

CORLESS, R. M. & JEFFREY, D. J. 1988 Stress moments of nearly touching spheres in low Reynolds number flow. *Z. Angew. Math. Phys.* **39**, 874–884.

DICKINSON, E. 1985 Brownian dynamics with hydrodynamic interactions: The application to protein diffusion problems. *Chem. Soc. Rev.* **14**, 421–455.

DURLOFSKY, L., BRADY, J. F. & BOSSIS, G. 1987 Dynamic simulation of hydrodynamically interacting particles. *J. Fluid Mech.* **180**, 21–49.

EVESON, G. F. 1959 *The Viscosity of Stable Suspensions of Spheres at Low Rates of Shear Appearing in Rheology of Disperse Systems.* Pergamon.

FARRIS, K. J. 1968 Prediction of the viscosity of multimodal suspensions from unimodal viscosity data. *Trans. Soc. Rheol.* **12**, 281–301.

GADALA-MARIA, F. A. 1979 The rheology of concentrated suspensions. PhD thesis, Stanford University.

GOTO, H. & KUNO, H. 1982 Flow of suspensions containing particles of two different sizes through a capillary tube. *J. Rheol.* **26**, 387–398.

GOTO, H. & KUNO, H. 1984 Flow of suspensions containing particles of two different sizes through a capillary tube. 2. Effect of the particle size ratio. *J. Rheol.* **28**, 197–205.

HOFFMAN, R. L. 1992 Factors affecting the viscosity of unimodal and multimodal colloidal dispersions. *J. Rheol.* **36**, 947–965.

JEFFREY, D. J. 1989 Stresslet resistance functions for low Reynolds number flow using deforming spheres. *Z. Angew. Math. Phys.* **40**, 163–171.

JEFFREY, D. J. 1992 The extended resistance functions for two unequal rigid spheres in low-Reynolds-number flow. *Phys. Fluids* A **4**, 16–29.

JEFFREY, D. J. & CORLESS, R. M. 1988 Forces and stresslets for the axisymmetric motion of nearly touching unequal spheres. *Physicochem. Hydrodyn.* **10**, 461–470.

JEFFREY, D. J. & ONISHI, Y. 1984 Calculation of the resistance and mobility functions for two unequal rigid spheres in low-Reynolds-number flow. *J. Fluid Mech.* **139**, 260–290.

JOMHA, A. I., MERRINGTON, A., WOODCOCK, L. V., BARNES, H. A. & LIPS, A. 1991 Recent developments in dense suspension rheology. *Powder Technol.* **65**, 343–370.

KAUSEH, H. H., FESKO, D. G. & TSCHOEGL, N. W. 1971 The random packing of circles in a plane. *J. Colloid Interface Sci.* **37**, 603–611.

KIM, S. & KARRILA, S. J. 1991 *Microhydrodynamics: Principles and Selected Applications.* Butterworth-Heinemann.

LEE, D. I. 1970 Packing of spheres and its effects on the viscosity of suspensions. *J. Paint Technol.* **42**, 579–587.

MCGEARY, R. K. 1961 Mechanical packing of spherical particles. *J. Am. Ceram. Soc.* **44**, 513–522.

MILLER, R. R., LEE, E. & POWELL, R. L. 1991 Rheology of solid propellant dispersions. *J. Rheol.* **35**, 901–920.

O'BRIEN, R. W. 1979 A method for the calculation of the effective transport properties of suspensions of interacting particles. *J. Fluid Mech.* **56**, 401–427.

PATTON, T. C. 1979 *Paint Flow and Pigment Dispersion.* John Wiley & Sons, New York, p. 150.

PÄTZOLD, R. 1980 Die Abhängigkeit des Fließverhaltens konzentrierter Kugelsuspensionen von der Strömungsform: Ein Vergleich der Viskosität in Scher- und Dehnströmungen. *Rheol. Acta* **19**, 322–344.

POSLINSKI, A. J., RYAN, M. E., GUPTA, P. K., SESHADRI, S. G. & FRECHETTE, F. J. 1988 Rheological behavior of filled polymeric systems. 2. The effect of a bimodal size distribution of particulates. *J. Rheol.* **32**, 751–771.

REED, T. M. & GUBBINS, K. E. 1973 *Applied Statistical Mechanics.* McGraw-Hill.

RUTGERS, R. 1962 Relative viscosity of suspensions of rigid spheres in Newtonian liquids. *Rheol. Acta* **2**, 202–210.

SENGUN, M. Z. & PROBSTEIN, R. F. 1989*a* Bimodal model of slurry viscosity with application to coal-slurries. Part 1. Theory and experiment. *Rheol. Acta* **28**, 382–393.

SENGUN, M. Z. & PROBSTEIN, R. F. 1989*b* Bimodal model of slurry viscosity with application to coal-slurries. Part 2. High shear limit behavior. *Rheol. Acta* **28**, 394–401.

SHAPIRO, A. P. & PROBSTEIN, R. F. 1992 Random packings of spheres and fluidity limits of monodisperse and bidisperse suspensions. *Phys. Rev. Lett.* **68**, 1422–1425.

STORMS, R. F., RAMARAO, B. V. & WEILAND, R. H. 1990 Low shear rate viscosity of bimodally dispersed suspensions. *Powder Technol.* **63**, 247–259.

SWEENY, K. H. & GECKLER, R. D. 1954 The rheology of suspensions. *J. Appl. Phys.* **25**, 1135–1144.

VISSCHER, W. M. & BOLSTERLI, M. 1972 Random packing of equal and unequal spheres in two and three dimensions. *Nature* **239**, 504–507.

WEINBAUM, S., GANATOS, P. & YAN, Z. Y. 1990 Numerical multipole and boundary integral equation techniques in Stokes flow. *Ann. Rev. Fluid Mech.* **22**, 275–316.